



# Application of fractional-order active disturbance rejection controller on linear motion system

Xinxin Shi <sup>a,\*</sup>, YangQuan Chen <sup>b</sup>, Jiakai Huang <sup>a</sup>

<sup>a</sup> School of Automation, Nanjing Institute of Technology, No. 1 Hongjing Road, Nanjing 211167, PR China

<sup>b</sup> Mechatronics, Embedded Systems and Automation Lab (MESA Lab), School of Engineering, University of California, Merced, CA 95343, USA



## ARTICLE INFO

### Keywords:

Fractional calculus  
Active disturbance rejection control  
Mechatronics  
Linear motors  
Motion control

## ABSTRACT

A fractional-order active disturbance rejection control strategy is presented to realize precise trajectory tracking and point-to-point positioning performances of a newly designed linear motor. Structure characteristics and working mechanism of the new linear motor are analyzed. Reference acceleration feedforward, extended state observer, tracking differentiator, and fractional-order proportional derivative algorithm are combined to achieve high-precision trajectory tracking and point-to-point positioning performances. Different simulations and experiments are compared, and results illustrate that the proposed method performs well in spite of parameter variations and external disturbances. Consequently, precision trajectory tracking and point-to-point positioning performances of the novel linear motor have been obtained.

## 1. Introduction

In modern industry, high-performance linear motions are widely needed, such as microchip manufacturers, industrial robots, and numerical control machines (Hu, Hu, Yu, & Wang, 2017; Itagaki & Tsutsumi, 2014; Zheng, Wang, Man, Jin, & Fu, 2015). Linear motors are potential suitable actuators for these applications for their simple structures and high-quality linear motion performances, especially in ultra-positioning system (Zhu, Chu, Yuan, Zhong, Zhao, & Gao, 2016), medical assistant robot (Chrif, Nef, Lungarella, Dravid, & Hunt, 2017), dual-linear-motor-driven gantry system (Li, Li, Chen, & Yao, 2018), and the 6-degree-of-freedom parallel platform (Shi, Chang, & Huang, 2014). Nevertheless, the control of the linear motor is usually difficult since the system can be easily influenced by uncertainties and disturbances such as parameter variations, friction, and ripple forces (Cheema, Fletcher, Xiao, & Rahman, 2016; Lin & Li, 2015; Lopez, Sanchez, Alanis, & Rios, 2017).

Linear motors are the most crucial elements in linear motion control systems, which have been designed with various structures (Baronti, Lazzeri, Saletti, & Saponara, 2013; Fu & Xu, 2017; Zhang, Wu, Liu, & Ding, 2013). This paper presents a new linear motor which has an ironless core to reduce ripple forces (Shi, Huang, & Li, 2016). Meanwhile, high performance permanent magnets (PMs) with neodymium iron boron (NdFeB) are arranged in the Halbach way to obtain enhanced air-gap flux density (Lee, Lee, & Gweon, 2004). Essentially, the new linear motor in this paper is a brushless, moving coil, tubular, direct current, and permanent magnet linear motor.

Precision trajectory tracking control and point-to-point positioning control are two important control tasks for linear motors (Chen & Lu,

2014; Hama & Sato, 2015). For one thing, precision trajectory tracking controls are usually used in continuous motion occasions (Lin & Chang, 2017). For example, metal materials are cut along given trajectories in numerical control machines. For another thing, precise point-to-point positioning controls are also needed such as industrial pick-and-place robots (Pellicciari, Berselli, Leali, & Vergnano, 2013). To achieve these control goals, the aforementioned uncertainties and disturbances should be handled well.

To achieve precision trajectory tracking performances, a motion trajectory generator can be used first and then a controller is designed to track it. Besides, an iterative learning control (ILC) can be used to realize good trajectory tracking performance when the motion is repetitive (Fu, Gu, Gu, & Wu, 2016; Naso, Cupertino, & Turchiano, 2010). For precise point-to-point positioning requirement, the time-optimal control (TOC) can be used to achieve this goal with minimal time (Shi & Chang, 2013). Another typical and effective controller is the adaptive robust control (ARC) (Hu, Yao, & Wang, 2013; Lu, Chen, Yao, & Wang, 2013), where system uncertainties and disturbances are handled on line by parameter adaptation and robust control algorithms.

Active disturbance rejection controller (ADRC) is an effective and practical controller which is firstly designed by Han (2009) and Huang and Xue (2014). There is no need to know system models accurately for ADRC since uncertainties and disturbances are estimated and therefore compensated on line (Gao, 2014; Sun, Hua, Li, Pan, Xue, & Lee, 2017). In addition, some other mechanisms are used to improve the precision motion control ability of the ADRC (Ran, Wang, Dong, Hou, & Wang, 2017; Xing, Jeon, Park, & Oh, 2013), such as feedforward control.

\* Corresponding author.

E-mail address: [sxx@njit.edu.cn](mailto:sxx@njit.edu.cn) (X. Shi).

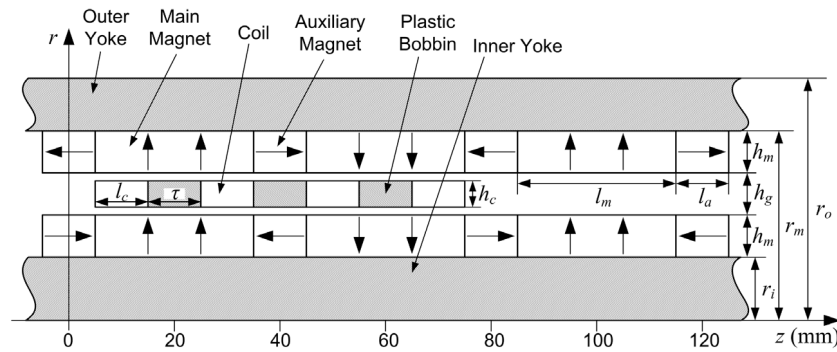


Fig. 1. Structure and mechanism of the new linear motor.

ADRC can be used to stabilize a class of uncertain nonlinear systems subject to stochastic disturbance (Guo, Wu, & Zhou, 2016), and it is suitable for different applications, such as air–fuel ratio control in gasoline engines (Xue, Bai, Yang, Song, Huang, & Xie, 2015), the ALSTOM gasifier benchmark problem (Huang, Li, & Xue, 2013), and active suspension system of tracked vehicles with gun (Xia, Fu, Li, Pu, & Xu, 2018).

Friction is an unneglected phenomenon, which is especially important for precision motion control, such as low-speed motions and speed-reverse points. LuGre model is widely used for imitating and compensating the actual action of friction force (Lu, Yao, Wang, & Chen, 2009). However, the friction model accuracy decides the compensation effect directly. Fractional-order control can be used to deal with these problems, which attracts more and more attention of the motion control field (Luo & Chen, 2013). Since the real complex phenomena are mostly fractional, the fractional calculus can be combined with conventional controllers to enhance control performances of systems.

A fractional-order proportional–integral–derivative (PI<sup>λ</sup>D<sup>μ</sup>) controller was designed in Zheng, Luo, Wang, Pi, and Chen (2017) to obtain satisfied performances in both frequency and time domains. In linear time-varying systems, an iterative learning control (ILC) was combined with fractional calculus to solve corresponding tracking problems (Zhao, Zhou, Wang, & Li, 2017). To improve the performance of linear fractional-order systems, a fractional active disturbance rejection control was designed, and comparative results showed the controller effectiveness (Li, Ding, & Gao, 2016). Fractional-order PD controllers derive from conventional PD controllers, in which the order of the derivative part is tunable. This tunable derivative order offers an additional control parameter which will improve the controller performance to an extent.

In this paper, a fractional-order active disturbance rejection controller (FOADRC) is proposed, in which the fractional-order PD is included. The proposed FOADRC is applied to a new linear motor motion control system. Compared with existing conventional technique, FOADRC has more tunable parameters and precision control performance can be achieved. Iterative learning process and on-line parameter adaptation will not be necessary while excellent disturbance rejection performance will be maintained. Precision trajectory tracking control and point-to-point positioning control strategies are designed based on FOADRC. The following three different controllers are compared: the conventional ADRC, the proportional–integral–derivative algorithm together with reference feedforward (PID + FF), and the presented FOADRC. Comparative results indicate that precision trajectory tracking control and point-to-point positioning performances of the new linear motor could be achieved by the proposed FOADRC.

The research goal of this paper is to find an effective controller which is simple to implement in real control engineering. Moreover, the designed linear motor has been used in a novel 6-degree-of-freedom parallel platform which is controlled by a modified active disturbance rejection controller (Shi et al., 2014). Therefore, the proposed FOADRC in this paper is expected to improve the control accuracy of this 6-degree-of-freedom parallel platform in the future.

Table 1  
Specifics of the linear motor.

Items	Symbols	Values (units: mm)
Main PM length	$l_m$	30
Auxiliary PM length	$l_a$	10
Coil length	$l_c$	10
Pitch of coil	$\tau$	10
Radius of inner yoke	$r_i$	10
PM width	$h_m$	6
Outer PM radius	$r_m$	27
Outer yoke radius	$r_o$	36
Air gap width	$h_g$	5
Coil width	$h_c$	3.7

## 2. Working principle analysis of a novel linear motor

### 2.1. Structure and mechanism

Here, a new linear motor was designed and assembled by authors to carry out the application study of the designed FOADRC. This linear motor is assembled by moving coils and quasi-Halbach magnet arrays, which is essentially a direct current (DC) motor without a brush.

Structure and mechanism of the new linear motor is demonstrated in Fig. 1, and dimensions of the self-fabricated prototype are presented in Table 1. It can be inferred from Fig. 2 that the trapezoidal distribution of air-gap magnetic field is obtained approximately.

### 2.2. Working process analysis

There are two phases in the linear motor. Windings A and X are linked serially to constitute phase 1 with opposite twining directions. In the same way, windings B and Y are also linked to form phase 2.

Fig. 3(a) shows the starting position, where phase 1 is powered on, the resulting electromagnetic force pushes the mover to motion constantly. Fig. 3(b) shows the commutation position, where phase 2 is powered on and phase 1 is powered off. Since the direction of the generated electromagnetic force is not change, the mover moves along the axis in the same direction as before.

### 2.3. Mathematical model

The linear motor system consists of two subsystems: mechanical ( $\Sigma x$ ) and electrical ( $\Sigma i$ ), which is expressed as

$$\begin{cases} F = F_f + F_r + F_d \\ \ddot{x} = -\frac{F}{m} + \frac{K_f}{m}i \quad (\Sigma x) \\ \dot{i} = -\frac{R}{L}i - \frac{K_e}{L}\dot{x} + \frac{1}{L}u \quad (\Sigma i), \end{cases} \quad (1)$$

where  $F_f$  denotes friction force,  $F_r$  denotes ripple force,  $F_d$  denotes external disturbances, and  $F$  denotes total uncertainties,  $m$  denotes the

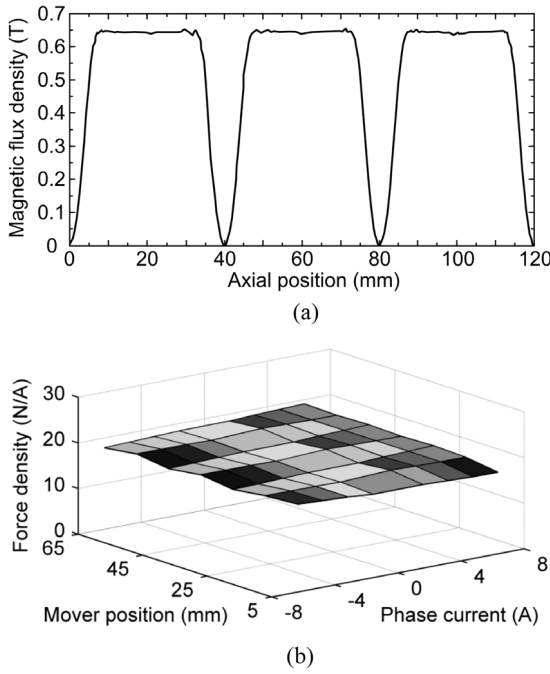


Fig. 2. Analysis results with finite elements of the new linear motor. (a) Air-gap magnetic field distribution. (b) Relationship between force, position, and current.



Fig. 3. Working process analysis. (a) Starting position. (b) Commutation position.

mover mass,  $x$  denotes the position,  $K_f$  represents the thrust constant,  $i$  represents phase current,  $K_c$  denotes back-electromotive-force (EMF) constant, phase resistance and phase inductance are represented by  $R$  and  $L$ , and  $u$  represents the input phase voltage.

### 2.4. Characteristics analysis

Characteristics of the linear motor are summarized as follows

- (1) Air-gap magnetic field distribution is trapezoidal as illustrated in Fig. 2, and the electromagnetic force is proportional to the phase current without respect to the mover position, which is easy to realize precision motion control.
- (2) Epoxy materials are used in linear motors herein to eliminate the cogging force effectively compared with their iron-core counterparts, and twining directions of two coils in each phase are opposite which will not affect the air-gap magnetic field obviously.

- (3) Like voice coil motors, operation principle of the linear motor is simple without coordinate transformation, while longer stroke can be achieved herein with the help of modular structures and commutations.

### 3. Precision linear motor motion control system design using FOADRC

The proposed FOADRC is composed of a reference acceleration feedforward (FF), a particular extended state observer (ESO), a preliminary tracking differentiator (TD), and a fractional-order proportional-derivative algorithm (FOPD).

FF, ESO, TD and FOPD are important components of the existing method FOADRC, and each part has its own function. FF provides a reference acceleration feedforward of the desired trajectory, which will improve tracking accuracy obviously. ESO is an extended state observer to observe total disturbances acting on the control system, which is the key part for excellent disturbances rejection. TD is used to generate pre-planned and smooth transitional processes of desired trajectories and positions, which can also improve the control accuracy to an extent. FOPD is the fractional-order PD controller, which has an additional tunable derivative order compared with the conventional PD controller. All these four parts constitute the FOADRC, and the whole system can work well.

#### 3.1. Detailed analysis of the FOADRC

TD is used to generate a pre-planned transitional process of the desired trajectory and position, which is discretized as follows:

$$\begin{cases} x_1(k+1) = x_1(k) + h \cdot x_2(k) \\ x_2(k+1) = x_2(k) + h \cdot \text{fhan}(x_1(k) - x_d(k), x_2(k), r, h_0), \end{cases} \quad (2)$$

where  $h$  represents the control period,  $k$  denotes the sampling instant,  $x_d$  denotes the desired position,  $x_1$  is the generated pre-planned transitional process of  $x_d$ ,  $x_2$  is the differential of  $x_1$ .  $\text{fhan}(x_1(k) - x_d(k), x_2(k), r, h_0)$  represents a nonlinear function with the expression as

$$\text{fhan}(x_1(k) - x_d(k), x_2(k), r, h_0) = \begin{cases} -r \cdot \text{sign}(a), & |a| > d \\ -r \cdot \frac{a}{d}, & |a| \leq d, \end{cases} \quad (3)$$

where  $r$  and  $h_0$  are function parameters,  $a$  and  $d$  are symbols which are defined as the following:

$$\begin{cases} d = r \cdot h_0 \\ d_0 = h_0 \cdot d \\ y_0 = x_1(k) - x_d(k) + h_0 \cdot x_2(k) \\ a_0 = \sqrt{d^2 + 8r \cdot |y_0|} \\ a = \begin{cases} x_2(k) + \frac{(a_0-d)}{2} \cdot \text{sign}(y_0), & |y_0| > d_0 \\ x_2(k) + \frac{y_0}{h_0}, & |y_0| \leq d_0. \end{cases} \end{cases} \quad (4)$$

ESO is used to observe total disturbances acting on the control system, and the second-order ESO is discretized with the sampling period  $h$  as follows:

$$\begin{cases} e = z_1(k) - x(k) \\ z_1(k+1) = z_1(k) + h \cdot (z_2(k) - \beta_{01} \cdot e) \\ z_2(k+1) = z_2(k) + h \cdot (z_3(k) - \beta_{02} \cdot \text{fal}(e, 0.5, \delta) + b \cdot u(k)) \\ z_3(k+1) = z_3(k) - h \cdot \beta_{03} \cdot \text{fal}(e, 0.25, \delta), \end{cases} \quad (5)$$

where  $b$  is a system parameter,  $k$  is the  $k$ th sampling instant,  $z_1$  is the output estimate  $x$ ,  $z_2$  estimates the derivative of  $x$ , and  $z_3$  is the estimate of the total disturbance.  $\beta_{01}$ ,  $\beta_{02}$ , and  $\beta_{03}$  are observer gains, and they can be established as follows:

$$\beta_{01} \approx \frac{1}{h}, \quad \beta_{02} \approx \frac{1}{1.6h^{1.5}}, \quad \beta_{03} \approx \frac{1}{8.6h^{2.2}}. \quad (6)$$

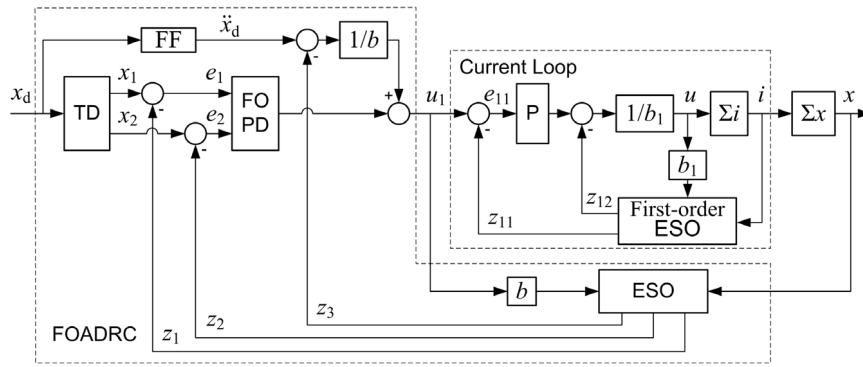


Fig. 4. Precision linear motor motion control design using FOADRC.

Table 2  
Specific parameter values of designed linear motor.

Parameters	Values
Resistance of phase ( $R$ )	3.4 $\Omega$
Inductance of phase ( $L$ )	4.42 mH
Moving mass ( $m$ )	250 g
Force coefficient ( $K_f$ )	18.01 N/A
Back EMF coefficient ( $K_e$ )	18.01 Vs/m
Total stroke	100 mm

The definition of the nonlinear function  $\text{fal}(e, \alpha, \delta)$  is given as

$$\text{fal}(e, \alpha, \delta) = \begin{cases} e \cdot \delta^{\alpha-1}, & |e| \leq \delta \\ |e|^\alpha \cdot \text{sign}(e), & |e| > \delta, \end{cases} \quad (7)$$

where the parameter  $\alpha$  satisfies the condition of  $\alpha < 1$  and the parameter  $\delta$  satisfies the condition of  $\delta = j \cdot h$ , where  $j$  is a positive integer.

Transfer function expression of FOPD is

$$C(s) = K_p(1 + K_d s^\mu), \quad (8)$$

where  $K_p$  and  $K_d$  are controller parameters,  $s$  is the Laplace variable,  $\mu$  is a real number which satisfies the condition  $0 < \mu < 1$ .

### 3.2. Precision linear motor motion control system design

Precision linear motor motion control system using FOADRC is designed as illustrated in Fig. 4. This whole control system consists of two loops: position loop and current loop. FOADRC is used in the position control loop, and first-order ESO is implemented in the current loop, which is discretized with the sampling period  $h_1$  as follows:

$$\begin{cases} e = z_{11}(k) - i(k) \\ z_{11}(k+1) = z_{11}(k) + h_1 \cdot (z_{12}(k) - \beta_{11} \cdot e + b_1 \cdot u(k)) \\ z_{12}(k+1) = z_{12}(k) - h_1 \cdot \beta_{12} \cdot \text{fal}(e, 0.5, \delta_1), \end{cases} \quad (9)$$

where  $z_{11}$  is the current estimate,  $z_{12}$  is total disturbance estimate of the electrical subsystem,  $b_1$  is a system parameter.  $\beta_{11}$ ,  $\beta_{12}$  and  $\delta_1$  are observer parameters, which can be established according to Eqs. (6)–(7).

## 4. Comparative simulations

Comparative simulations are implemented in Matlab/Simulink. LuGre model is adopted herein to simulate the friction dynamics, which is described in Wit, Olsson, Åström, and Lischinsky (1995). Table 2 shows specific parameter values of the new linear motor.

Three different controllers are compared as follows.

(1) ADRC: conventional ADRC is composed of a second-order ESO, a preliminary TD, and a particular nonlinear proportional-derivative (NPD) algorithm. NPD algorithm is given as

$$\begin{cases} e_1 = x_1 - z_1 \\ e_2 = x_2 - z_2 \\ u_0 = \beta_1 \cdot \text{fal}(e_1, \alpha_1, \delta) + \beta_2 \cdot \text{fal}(e_2, \alpha_2, \delta) \text{ (NPD)}, \end{cases} \quad (10)$$

where  $\beta_1$ ,  $\beta_2$ ,  $\alpha_1$ ,  $\alpha_2$ , and  $\delta$  are controller parameters. TD parameters:  $r$  is used to determine the transient process of  $x_d$  which will be given in Section 4.2,  $h_0 = 0.0002$ .

ESO parameters are:  $h = 0.0002$ ,  $\beta_{01} = 5000$ ,  $\beta_{02} \approx 220970$ ,  $\beta_{03} \approx 15967450$ ,  $\delta = 25 \times h = 0.005$ ,  $b \approx 72$  and NPD parameters are:  $\beta_1 = 30000$ ,  $\beta_2 = 10000$ ,  $\alpha_1 = 0.75$ ,  $\alpha_2 = 1.5$ ,  $\delta = 25 \times h = 0.005$ .

(2) PID+FF: conventional PID together with acceleration feedforward (FF). PI controller is used in the inner current loop, and PID algorithm is implemented in the outer position loop. Controller gains of PI are  $K_p = 150$ ,  $K_i = 10000$ , and PID gains are  $K_p = 34000$ ,  $K_i = 1000$ ,  $K_d = 100$ .

(3) FOADRC: as shown in Fig. 4. TD parameters are:  $r$  is used to determine the transient process of  $x_d$ , which will be given in Section 4.2,  $h_0 = 0.0002$ , ESO parameters in the position loop are:  $h = 0.0002$ ,  $\beta_{01} = 5000$ ,  $\beta_{02} \approx 220970$ ,  $\beta_{03} \approx 15967450$ ,  $b \approx 72$ , and  $\delta = h = 0.0002$ . FOPD gains are  $K_p = 100000$  and  $K_d = 300$ . The fractional order  $\mu$  is set as 0.835, and the finite order of the approximate z-transfer function is set as 5. Parameters of the first-order ESO are:  $\beta_{11} = 40000$ ,  $\beta_{12} \approx 5000000$ ,  $b_1 = 1/L \approx 226$ ,  $h_1 = 0.000025$ ,  $\delta_1 = h_1$ , and the inner current loop P controller parameter is  $K_p = 40000$ .

For the purpose of simulating the friction dynamics, LuGre model is adopted, which is given according to Wit et al. (1995).

$$F_f = \sigma_0 z + \sigma_1 \frac{dz}{dt} + \sigma_2 v, \quad (11)$$

where  $v$  is the velocity,  $\sigma_0$ ,  $\sigma_1$ , and  $\sigma_2$  are parameters, and  $z$  is given in Eq. (12)

$$\frac{dz}{dt} = v - \frac{|v|}{g(v)} z. \quad (12)$$

where  $g(v)$  is calculated by Eq. (13)

$$\sigma_0 g(v) = F_C + (F_S - F_C) e^{-(v/v_s)^2}, \quad (13)$$

where  $v_s$  indicates the Stribeck effect,  $F_C$  denotes the Coulomb force, and  $F_S$  denotes the stiction effect. Specific value of each parameter in LuGre friction model are given as  $(v_s, F_S, F_C, \sigma_0, \sigma_1, \sigma_2) = (0.001 \text{ m/s}, 1.5 \text{ N}, 1 \text{ N}, 10^5 \text{ N/m}, 10^{2.5} \text{ Ns/m}, 0.4 \text{ Ns/m})$  according to Wit et al. (1995).

### 4.1. Open-loop responses for different operating conditions

In order to study the open-loop performance of the system, open-loop responses for different operating conditions have been illustrated in Fig. 5. Input voltages are given as follows.

$$u = \begin{cases} \sin \pi t \text{ (V)}, & U1 \\ \sin 2\pi t \text{ (V)}, & U2 \end{cases} \quad (14)$$

Here, the following three different operating conditions are considered. (a) Without payload; (b) With payload, that is, the system parameter  $m$  varies from 0.25 kg to 16 kg; (c) With disturbance, that is, at  $t = 0.4 \text{ s}$  the disturbance  $F_d = -1 \text{ N}$  is imposed on the system and at  $t = 1.1 \text{ s}$  the disturbance is removed.

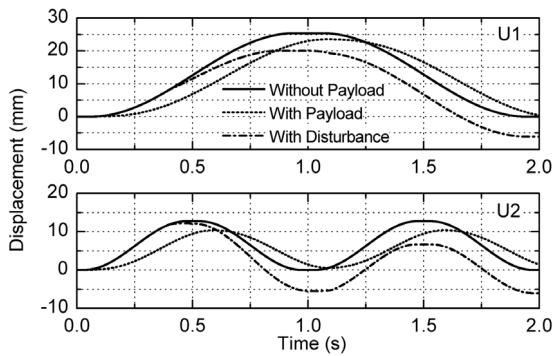


Fig. 5. Open-loop responses for different operating conditions.

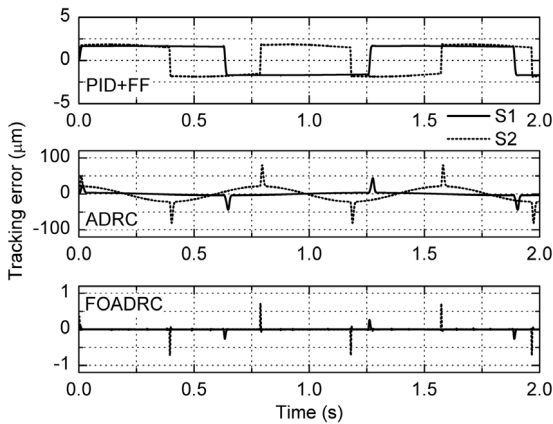


Fig. 6. Comparative results for different trajectories without payload.

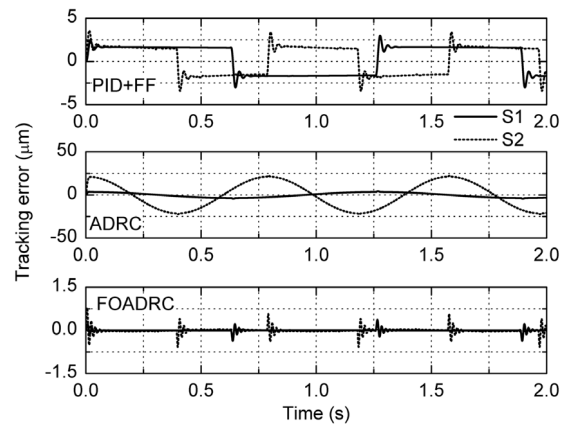


Fig. 7. Comparative results for different trajectories with payload.

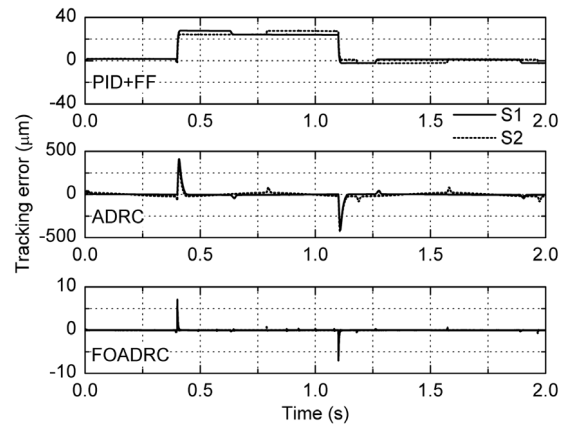


Fig. 8. Comparative results for different trajectories with disturbances.

#### 4.2. Trajectory tracking control tasks comparisons

Two sinusoidal curves are established as the desired trajectories, expressions of which are given as follows.

$$x_d = \begin{cases} 15 \sin(5t - 0.5\pi) + 15 \text{ (mm)}, & S1 \\ 35 \sin(8t - 0.5\pi) + 35 \text{ (mm)}, & S2 \end{cases} \quad (15)$$

Trajectory tracking motion control comparative results under the aforementioned three different controllers are illustrated in Fig. 6, and it indicates that the proposed FOADRC tracks the desired trajectories well and therefore high-precision motion performances are achieved.

In addition, a 15.75 kg payload is added on the control system to check whether the controller is robust to parameter variations, that is, the system parameter  $m$  varies from 0.25 kg to 16 kg. Fig. 7 shows the comparative simulations.

It can be seen obviously from Fig. 7 that the FOADRC is very robust to parameter variations compared with two other controllers.

Moreover, an external disturbance is added. That is, at  $t = 0.4$  s the disturbance  $F_d = -16$  N is imposed on the system and at  $t = 1.1$  s the disturbance is removed. Comparative simulations are illustrated in Fig. 8.

It is illustrated in Fig. 8 that the presented FOADRC is robust and the disturbance rejection performance is good. Figs. 6–8 show that compared with two other controllers, FOADRC is robust to both parameter uncertainties and external disturbances, and precision trajectory tracking performance of the new linear motor motion control system has been achieved.

#### 4.3. Point-to-point positioning control tasks comparisons

Two desired positions are  $x_d = 12$  mm and 28 mm, respectively. The reference acceleration feedforward is given as

$$\ddot{x}_d = \begin{cases} r, & 0 \leq t \leq 0.1 \text{ s} \\ -r, & 0.1 < t \leq 0.2 \text{ s (m/s}^2\text{)} \\ 0, & t > 0.2 \text{ s} \end{cases} \quad (16)$$

Here,  $r$  is selected as 1.2 for the desired position  $x_d = 12$  mm and 2.8 for the desired position  $x_d = 28$  mm, respectively. Comparative motion control results under aforementioned three different methods are illustrated in Fig. 9, and the proposed FOADRC tracks the planned transient process well and therefore high-precision positioning performance is achieved.

Similar to the trajectory tracking control, an additional payload as 15.75 kg is put on the system to test the controller robustness to parameter variations, and therefore the parameter  $m$  varies from 0.25 kg to 16 kg. Comparative results are illustrated in Fig. 10. It is indicated that the FOADRC controller performs well under parameter variations compared with two other controllers.

Moreover, an external disturbance  $F_d = -12$  N is added on the system at  $t = 0.3$  s and taken away at  $t = 0.4$  s. Controller performances under external disturbances are compared in Fig. 11.

Fig. 11 shows that the proposed FOADRC is robust and disturbance rejection performance is good. Figs. 9–11 show that precision point-to-point positioning performance of the FOADRC has been obtained even in the present of either parameter uncertainties or uncertain external disturbances.

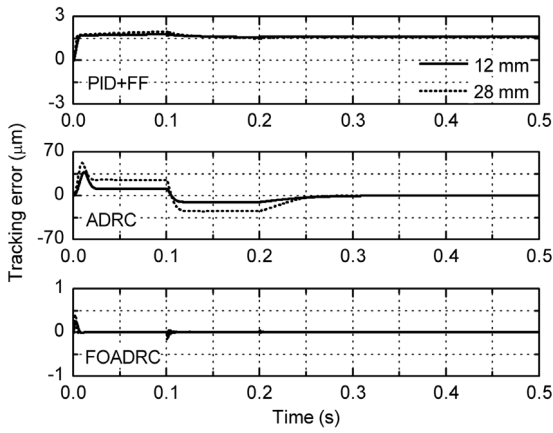


Fig. 9. Comparative positioning performances for different desired positions without payload.

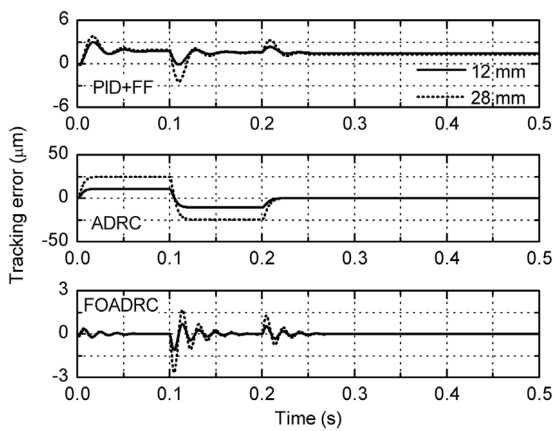


Fig. 10. Comparative positioning performances with payload.

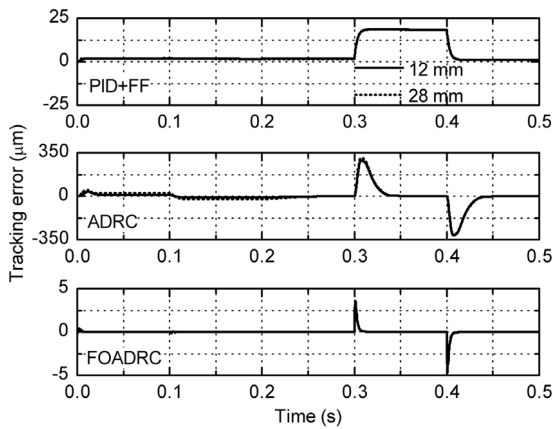
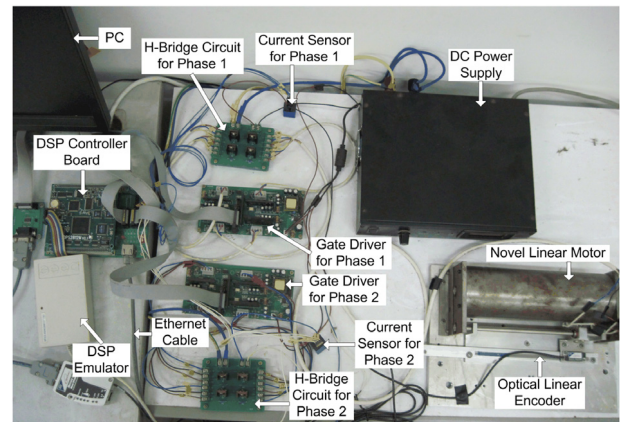


Fig. 11. Comparative positioning performances with disturbances.

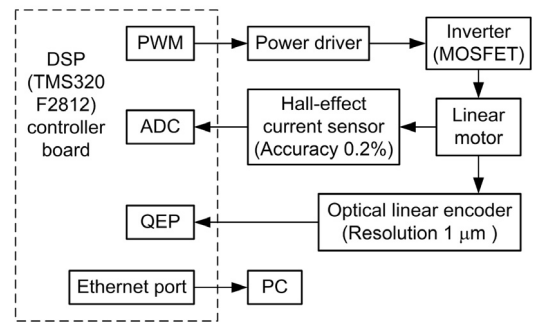
### 5. Experiments

Experiments were carried out on a linear motor prototype to verify the actual motion control performance of the presented FOADRC in control engineering practice. Actual experimental setup based on digital signal processor (DSP) is illustrated in Fig. 12.

Hall-effect current sensors with accuracy 0.2% and the optical linear encoder with resolution 1 µm were used to measure phase currents and the mover position respectively, and output signals were connected

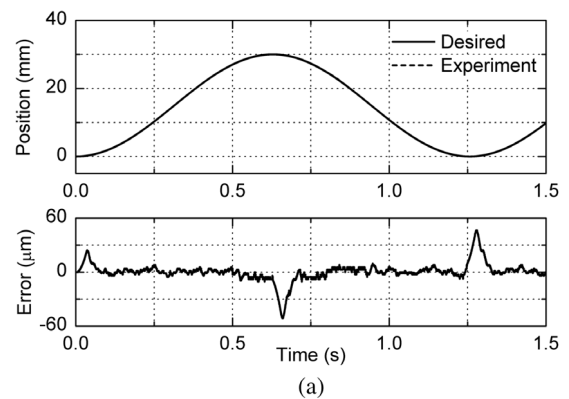


(a)

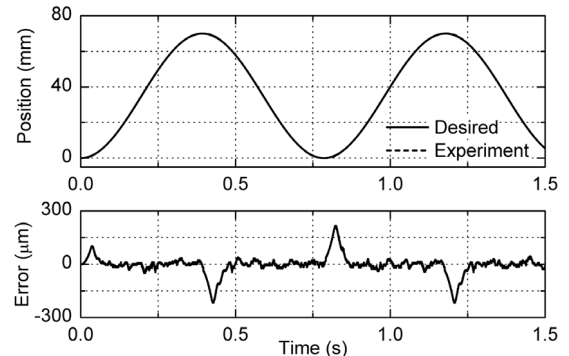


(b)

Fig. 12. Experimental setup for control performance validation. (a) Actual construction. (b) Schematic diagram.



(a)



(b)

Fig. 13. Experimental results of linear motor trajectory tracking system based on FOADRC. (a) sinusoidal trajectory No. 1 (S1). (b) sinusoidal trajectory No.2 (S2).

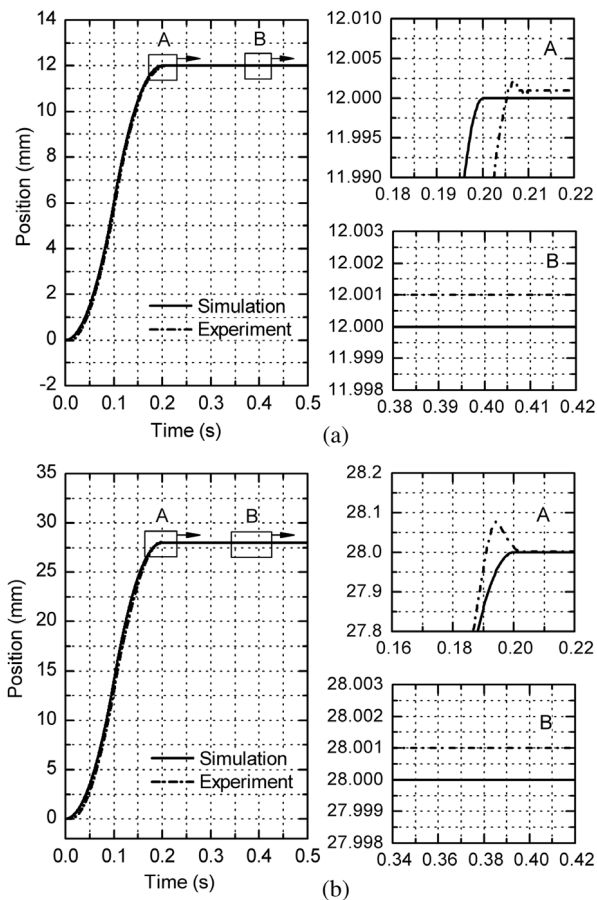


Fig. 14. Experimental results of linear motor point-to-point positioning system based on FOADRC. (a) desired position No. 1 (12 mm). (b) desired position No. 2 (28 mm).

to the analog-to-digital converter (ADC) and quadrature-encoder pulse (QEP) units of the DSP respectively. Pulse-width modulation (PWM) signals were generated and used to drive the metallic-oxide-semiconductor-field-effect transistor (MOSFET) inverter to realize power amplification.

The position sampling period was set as 0.2 ms, and the current loop sampling period was 0.025 ms. Experimental data were displayed and analyzed on the personal computer (PC) which were transmitted by an Ethernet cable.

Experimental results are illustrated in Figs. 13–14. Fig. 13 demonstrates that the proposed FOADRC also performs well in practice, and tracking errors are less than 20  $\mu\text{m}$  except for speed-reverse points. Positioning errors are illustrated in Fig. 14, which are within 1  $\mu\text{m}$ , and the resolution of the position sensor is also 1  $\mu\text{m}$ .

Moreover, since the DSP TMS320F2812's calculation capability and sensors' measuring accuracies are limited, there are some differences between simulation and actual measurement results. In addition, similar to simulations, there are some spikes in motion curves which are mainly the results of the friction action.

## 6. Conclusions

A fractional-order active disturbance rejection controller (FOADRC) is presented to realize desired motion control performances of a newly designed linear motor, including trajectory tracking control and point-to-point positioning control. FOADRC is composed of a reference acceleration feedforward, an extended state observer, a tracking differentiator, and a fractional-order proportional-derivative controller. Advantages of the fractional-order active disturbance rejection control in existing research are more tunable parameters, simple realization and

operation, robustness to disturbances, and high tracking and positioning accuracy. Meanwhile, problems of the FOADRC are that there are many parameters need to be established, and the desired trajectories or positions need to be known accurately in advance. Comparative simulations and various experiments are carried out to validate the control performance of the presented FOADRC, which can achieve precision trajectory tracking and point-to-point positioning performances in spite of system parameter variations and external disturbances. The major contribution of the paper is the precision motion control of a newly designed linear motor, and this linear motor together with the proposed FOADRC control strategy provides an additional solution for precision linear motion control engineering applications.

## Acknowledgments

This work was supported by the National Natural Science Foundation of China [grant number 51505213]; the Natural Science Foundation of Jiangsu Province, China [grant number BK20151463]; and the Jiangsu Government Scholarship for Overseas Studies [grant number JS-2016-001]. The authors would like to express their appreciation to the sponsors.

## Declaration of conflict interests

The authors declared no potential conflicts of interest with respect to the research, authorship, and/or publication of this article.

## References

- Baronti, F., Lazzeri, A. R. R., Saletti, R., & Saponara, S. (2013). Design and characterization of a robotized gearbox system based on voice coil actuators for a formula sae race car. *IEEE/ASME Transactions on Mechatronics*, 18, 52–61.
- Cheema, M. A. M., Fletcher, J. E., Xiao, D., & Rahman, M. F. (2016). A direct thrust control scheme for linear permanent magnet synchronous motor based on online duty ratio control. *IEEE Transactions on Power Electronics*, 31, 4416–4428.
- Chen, M. -Y., & Lu, J. -S. (2014). High-precision motion control for a linear permanent magnet iron core synchronous motor drive in position platform. *IEEE Transactions on Industrial Informatics*, 10, 99–108.
- Chrif, F., Nef, T., Lungarella, M., Dravid, R., & Hunt, K. J. (2017). Control design for a lower-limb paediatric therapy device using linear motor technology. *Biomedical Signal Processing and Control*, 38, 119–127.
- Fu, Q., Gu, W. -G., Gu, P. -P., & Wu, J. -R. (2016). Iterative learning control for a class of mixed hyperbolic-parabolic distributed parameter systems. *International Journal of Control, Automation and Systems*, 14, 1455–1463.
- Fu, D. -S., & Xu, Y. -L. (2017). Presentation of a novel E-core transverse-flux permanent magnet linear motor and its magnetic field analysis based on schwarz-christoffel mapping method. *Journal of Electrical Engineering and Technology*, 12, 1963–1969.
- Gao, Z. (2014). On the centrality of disturbance rejection in automatic control. *ISA Transactions*, 53, 850–857.
- Guo, B. -Z., Wu, Z. -H., & Zhou, H. -C. (2016). Active disturbance rejection control approach to output-feedback stabilization of a class of uncertain nonlinear systems subject to stochastic disturbance. *IEEE Transactions on Automatic Control*, 61, 1613–1618.
- Hama, T., & Sato, K. (2015). High-speed and high-precision tracking control of ultrahigh-acceleration moving-permanent-magnet linear synchronous motor. *Precision Engineering*, 40, 151–159.
- Han, J. (2009). From PID to active disturbance rejection control. *IEEE Transactions on Industrial Electronics*, 56, 900–906.
- Hu, C., Hu, Z., Yu, Z., & Wang, Z. (2017). Advanced GTCF-LARC contouring motion controller design for an industrial X-Y linear motor stage with experimental investigation. *IEEE Transactions on Industrial Electronics*, 64, 3308–3318.
- Hu, C., Yao, B., & Wang, Q. (2013). Performance-oriented adaptive robust control of a class of nonlinear systems preceded by unknown dead zone with comparative experimental results. *IEEE/ASME Transactions on Mechatronics*, 18, 178–189.
- Huang, C. -E., Li, D., & Xue, Y. (2013). Active disturbance rejection control for the ALSTOM gasifier benchmark problem. *Control Engineering Practice*, 21, 556–564.
- Huang, Y., & Xue, W. (2014). Active disturbance rejection control: Methodology and theoretical analysis. *ISA Transactions*, 53, 963–976.
- Itagaki, H., & Tsutsumi, M. (2014). Control system design of a linear motor feed drive system using virtual friction. *Precision Engineering*, 38, 237–248.
- Lee, M. G., Lee, S. Q., & Gweon, D. G. (2004). Analysis of Halbach magnet array and its application to linear motor. *Mechatronics*, 14, 115–128.
- Li, D., Ding, P., & Gao, Z. (2016). Fractional active disturbance rejection control. *ISA Transactions*, 62, 109–119.

- Li, C., Li, C., Chen, Z., & Yao, B. (2018). Advanced synchronization control of a dual-linear-motor-driven gantry with rotational dynamics. *IEEE Transactions on Industrial Electronics*, *65*, 7526–7535.
- Lin, C. -Y., & Chang, C-Y. (2017). Repetitive model predictive control for precise control of complex trajectory tracking in dual-stage actuator systems. *Proceedings of the Institution of Mechanical Engineers Part I: Journal of Systems and Control Engineering*, *231*, 213–229.
- Lin, C. -M., & Li, H. -Y. (2015). Dynamic petri fuzzy cerebellar model articulation controller design for a magnetic levitation system and a two-axis linear piezoelectric ceramic motor drive system. *IEEE Transactions on Control Systems Technology*, *23*, 693–699.
- Lopez, V. G., Sanchez, E. N., Alanis, A. Y., & Rios, J. D. (2017). Real-time neural inverse optimal control for a linear induction motor. *International Journal of Control*, *90*, 800–812.
- Lu, L., Chen, Z., Yao, B., & Wang, Q. (2013). A two-loop performance-oriented tip-tracking control of a linear-motor-driven flexible beam system with experiments. *IEEE Transactions on Industrial Electronics*, *60*, 1011–1022.
- Lu, L., Yao, B., Wang, Q., & Chen, Z. (2009). Adaptive robust control of linear motors with dynamic friction compensation using modified LuGre model. *Automatica*, *45*, 2890–2896.
- Luo, Y., & Chen, Y. (2013). *Fractional order motion controls*. Chichester: John Wiley & Sons Ltd.
- Naso, D., Cupertino, F., & Turchiano, B. (2010). Precise position control of tubular linear motors with neural networks and composite learning. *Control Engineering Practice*, *18*, 515–522.
- Pellicciari, M., Berselli, G., Leali, F., & Vergnano, A. (2013). A method for reducing the energy consumption of pick-and-place industrial robots. *Mechatronics*, *23*, 326–334.
- Ran, M., Wang, Q., Dong, C., Hou, Y., & Wang, Z. (2017). Backstepping active disturbance rejection control: A delayed activation approach. *IET Control Theory & Applications*, *11*, 2336–2342.
- Shi, X., & Chang, S. (2013). Extended state observer-based time-optimal control for fast and precise point-to-point motions driven by a novel electromagnetic linear actuator. *Mechatronics*, *23*, 445–451.
- Shi, X., Chang, S., & Huang, J. (2014). Motion control of a novel 6-degree-of-freedom parallel platform based on modified active disturbance rejection controller. *Proceedings of the Institution of Mechanical Engineers Part I: Journal of Systems and Control Engineering*, *228*, 87–96.
- Shi, X., Huang, J., & Li, H. (2016). Extended state observer-based fractional order proportional-derivative controller for precision trajectory tracking control of a novel linear motor. *Proceedings of the Institution of Mechanical Engineers Part I: Journal of Systems and Control Engineering*, *230*, 95–103.
- Sun, L., Hua, Q., Li, D., Pan, L., Xue, Y., & Lee, K. Y. (2017). Direct energy balance based active disturbance rejection control for coal-fired power plant. *ISA Transactions*, *70*, 486–493.
- Wit, C. C. d., Olsson, H., Åström, K. J., & Lischinsky, P. (1995). A new model for control of systems with friction. *IEEE Transactions on Automatic Control*, *40*, 419–425.
- Xia, Y., Fu, M., Li, C., Pu, F., & Xu, Y. (2018). Active disturbance rejection control for active suspension system of tracked vehicles with gun. *IEEE Transactions on Industrial Electronics*, *65*, 4051–4060.
- Xing, H. L., Jeon, J. H., Park, K. C., & Oh, I. K. (2013). Active disturbance rejection control for precise position tracking of ionic polymer-metal composite actuators. *IEEE/ASME Transactions on Mechatronics*, *18*, 86–95.
- Xue, W., Bai, W., Yang, S., Song, K., Huang, Y., & Xie, H. (2015). ADRC with adaptive extended state observer and its application to air-fuel ratio control in gasoline engines. *IEEE Transactions on Industrial Electronics*, *62*, 5847–5857.
- Zhang, G., Wu, J., Liu, P., & Ding, H. (2013). Dynamic analysis and model-based feedforward control of a 2-dof translational parallel manipulator driven by linear motors. *Industrial Robot*, *40*, 597–609.
- Zhao, Y., Zhou, F., Wang, Y., & Li, Y. (2017). Fractional-order iterative learning control with initial state learning design. *Nonlinear Dynamics*, *90*, 1257–1268.
- Zheng, W., Luo, Y., Wang, X., Pi, Y., & Chen, Y. (2017). Fractional order  $PI^{\lambda}D^{\mu}$  controller design for satisfying time and frequency domain specifications simultaneously. *ISA Transactions*, *68*, 212–222.
- Zheng, J., Wang, H., Man, Z., Jin, J., & Fu, M. (2015). Robust motion control of a linear motor positioner using fast nonsingular terminal sliding mode. *IEEE/ASME Transactions on Mechatronics*, *20*, 1743–1752.
- Zhu, C., Chu, X., Yuan, S., Zhong, Z., Zhao, Y., & Gao, S. (2016). Development of an ultrasonic linear motor with ultra-positioning capability and four driving feet. *Ultrasonics*, *72*, 66–72.